Reflection and transmission of surface waves at a vertical discontinuity and imaging of lateral heterogeneity using reflected fundamental Rayleigh waves

Article *in* Bulletin of the Seismological Society of America · December 1997

CITATIONS
24

READS
119

3 authors, including:

Peter Malischewsky
Friedrich Schiller University Jena
70 PUBLICATIONS **791** CITATIONS

SEE PROFILE

Bulletin of the Seismological Society of America, Vol. 87, No. 6, pp. 1648–1661, December 1997

Reflection and Transmission of Surface Waves at a Vertical Discontinuity and Imaging of Lateral Heterogeneity Using Reflected Fundamental Rayleigh Waves

by T. Meier, P. G. Malischewsky, and H. Neunhöfer

Abstract We present a technique for the determination of approximate reflection and transmission coefficients of surface-wave modes for a vertical plane discontinuity that is simple to use. It is applied to different models of lateral heterogeneity. Furthermore, a method for the localization of lateral heterogeneity using the coda of the fundamental Rayleigh mode is proposed. In particular, the frequency content of surface waves enables the investigation of the lower crust and the uppermost mantle. Lateral changes of the *S*-wave velocity, density, and *P*-wave velocity lead to the formation of the coda of the fundamental Rayleigh mode that contains delayed surface waves that reach the recording station indirectly. The complicated structure of the coda makes it impossible to identify reflected surface waves visually using a small number of recordings only. Coda waveforms of a large number of source-station pairs are inverted simultaneously for experimental reflection coefficients. The method is successfully tested using an ultrasonic model experiment. Finally, it is applied to Central Europe and especially to the Tornquist zone (TZ), mainly using records of the German Regional Seismological Network (GRSN). The resulting reflection coefficients depend on frequency and give an image of the location of reflectors.

Introduction

The investigation of surface waves can yield useful information especially about the *S*-wave velocity structure of the crust and the upper mantle. Smooth and sharp lateral changes of the structure affect the propagation of surface waves. For example, Levshin (1985) discussed different factors that could influence surface waves in a laterally inhomogeneous medium. An indication of the presence of strong lateral changes is the existence of the surface-wave coda, which contains delayed surface waves that reach the recording station indirectly. The surface-wave coda can be studied for lateral heterogeneity. Aki and Chouet (1975) develop a statistical approach that is based on coda Q. Levshin and Berteussen (1979) use an array to determine directions of propagation of secondary surface waves within the coda. Snieder (1986, 1988) and Snieder and Nolet (1987) describe surface-wave scattering with the help of the Born approximation and develop an inversion scheme for *S*-wave velocity that is applied to the direct fundamental Rayleigh mode and the coda of the fundamental Rayleigh mode.

Here reflection and transmission at a vertical discontinuity are considered to describe the interaction of surface waves with strong and sharp lateral heterogeneity. First, a method for the approximation of reflection and transmission coefficients for a given discontinuity is discussed and applied to different discontinuities. Second, an attempt is made to determine reflection coefficients by inverting a large number of recordings simultaneously. A linear inversion is carried out to determine reflection coefficients that nonlinearly depend on the structural parameters. The method is tested by an ultrasonic experiment, and it is applied to Central Europe, especially to the Tornquist zone (TZ), by using broadband records of the German Regional Seismological Network (GRSN) (Hanka, 1990). In this analysis, we use the vertical components of reflected fundamental modes of Rayleigh waves.

Approximation of Reflection Coefficients for Surface Waves

Models with lateral changes that are abrupt in comparison to the wavelength of the surface waves are considered. Such models can be justified for certain geological structures, because the observed wavelengths of surface waves for frequencies lower than 50 mHz are larger than 50 km. Furthermore, we restrict ourselves to a plane vertical discontinuity between two layered quarter spaces and to plane waves.

Exact reflection and transmission coefficients for surface waves can be determined analytically for very few special cases only, for example, for the so-called Sato model (Sato, 1961) or by using the elaborate Wiener-Hopf technique, for an impedance jump on an impedance surface (Malischewsky, 1987). Furthermore, for closed wave guides, it is possible to find exact solutions by expanding into appropriate eigenfunctions (e.g., Stange and Friederich, 1992). For open wave guides with general discontinuities, approximation techniques have to be applied. Essentially, these techniques are based upon the Green's function method (e.g., Its and Yanovskaya, 1985; Keilis-Borok, 1989), the method of coupled modes (e.g., Kennett, 1984; Maupin and Kennett, 1987), or the so-called mode-matching techniques (Alsop, 1966). Gregersen and Alsop (1974) applied another method by exactly fulfilling the boundary conditions on the discontinuity but not on the free surface. Malischewsky (1979, 1987) proposed a criterion based upon the mode-matching technique for the estimation of the reflection and transmission coefficients. The criterion can be brought into a form well suited for programming, and it yields results that are in good agreement to the results presented by Its and Yanovskaya (1985). The criterion concerns incomplete eigenfunction sets and is in conformity with the theory of connectivity and biorthogonality. The range of validity of this approximation was extensively discussed by Malischewsky (1987) by using various simple test cases. In many cases, the results are encouraging; however, there is no rule of thumb for the general case.

We consider two quarter spaces (medium 1 and medium 2), welded along the plane $x_1 = 0$. The free surface is located at $x_3 = 0$. According to Malischewsky (1976), the cartesian components ($i = 1, 2, 3$) of the eigenfunctions (depending on frequency and depth x_3) may be written for the displacements as

$$U_i^\alpha = \begin{cases} \delta_{1i}U_1^\alpha + \delta_{3i}U_3^\alpha, & \alpha = 0, \ldots, M_m, \\ \delta_{2i}U_2^\alpha, & \alpha = M_m + 1, \ldots, N_m, \end{cases} \quad (1)$$

and analogously for the stresses as

$$S_{ij}^\alpha = \begin{cases} \delta_{i1}\delta_{j1}S_{11}^\alpha + \delta_{i2}\delta_{j2}S_{22}^\alpha + \delta_{i3}\delta_{j3}S_{33}^\alpha + \\ (\delta_{i1}\delta_{j3} + \delta_{i3}\delta_{j1})\, S_{13}^\alpha, \ \alpha = 0, \ldots, M_m, \\ (\delta_{i1}\delta_{j2} + \delta_{i2}\delta_{j1})\, S_{12}^\alpha + (\delta_{i2}\delta_{j3} + \delta_{i3}\delta_{j2})\, S_{23}^\alpha, \\ \alpha = M_m + 1, \ldots, N_m. \end{cases} \quad (2)$$

Here, m stands for medium 1 or 2 and α is the mode index. It runs over the Rayleigh modes ($\alpha = 0, \ldots, M_m$) and over the Love modes ($\alpha = M_m + 1, \ldots, N_m$) as well. For brevity, we drop the medium index at the eigenfunctions, but the index m in M_m and N_m refers to the medium under consideration. The components U_1^α and U_2^α are imaginary, and U_3^α is real. The behavior of the stress components is straightforward; especially S_{11} and S_{12} are real, and S_{13} is imaginary.

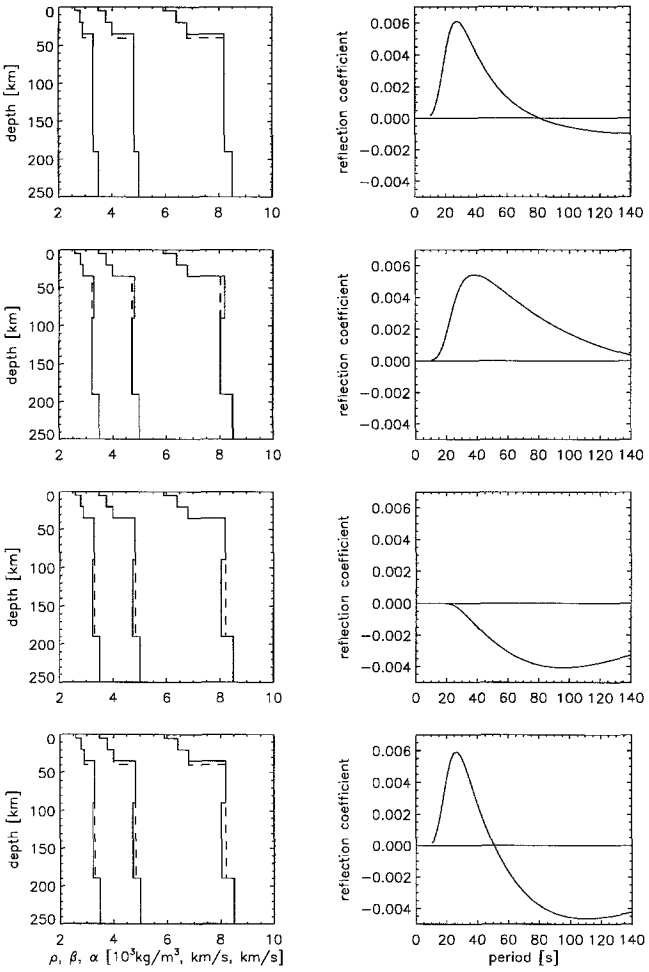

Figure 1. *Left:* Density, *S*- and *P*-wave velocity as a function of depth for two models at four vertical discontinuities (solid line, model 1; dashed line, model 2). *Right:* Reflection coefficient of the reflected fundamental Rayleigh mode as a function of period for perpendicular incidence of a fundamental Rayleigh mode.

For the calculation of the reflection and transmission coefficients, it is convenient to normalize the eigenfunctions according to

$$\frac{i\omega}{4}\int_0^\infty (U_j^\alpha S_{1j}^{\beta *} - U_j^{\beta *} S_{1j}^\alpha)\, dx_3 = \delta_{\alpha\beta}, \ \alpha,\beta = 0, \ldots, N_m. \quad (3)$$

The star denotes complex conjugation, and Einstein's convention is understood for the lower index. Here we assume that plane surface waves that transport unit energy are propagating into direction x_1. In this manner, the reflection and transmission coefficients refer to energy. In medium 1, a non-normally incident surface-wave mode is assumed, whose mode index is dropped for brevity. All horizontal

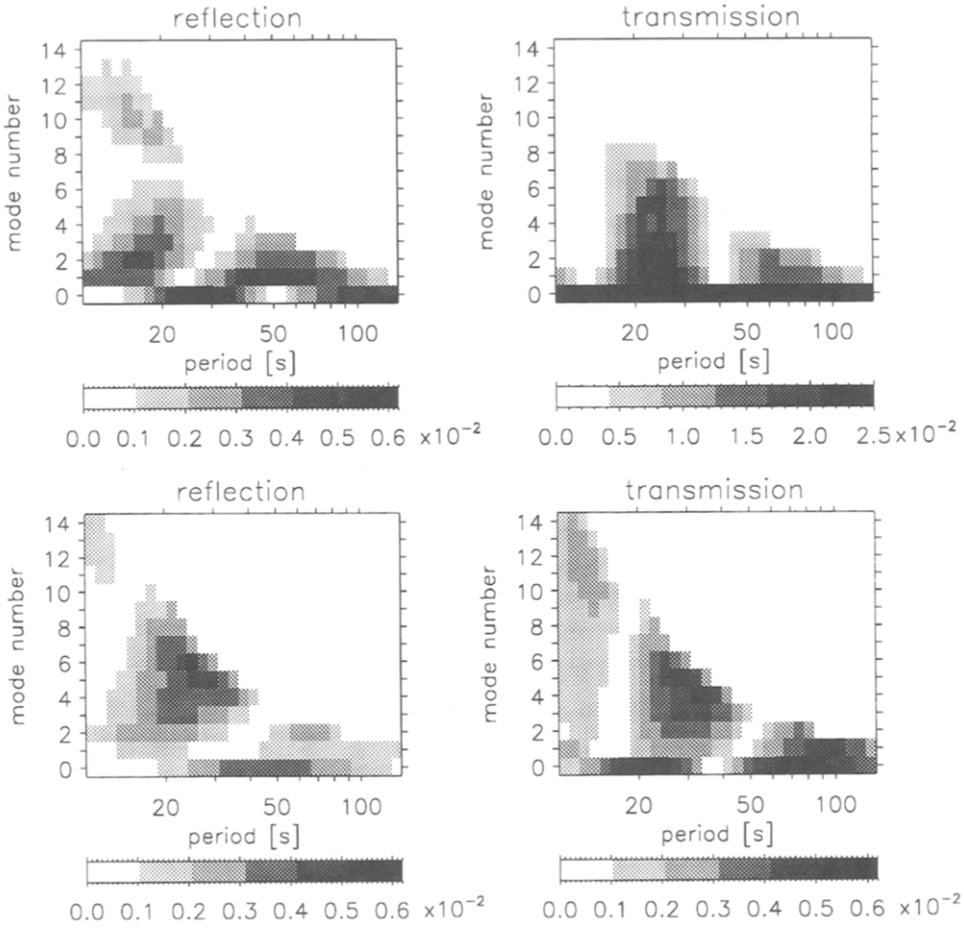

Figure 2. Absolute value of reflection and transmission coefficients as a function of period and mode number for the model in Figure 1 on the bottom left. *Top:* Reflected and transmitted Rayleigh modes for a perpendicularly incident fundamental Rayleigh mode. Absolute values of transmission coefficients of the fundamental Rayleigh mode are cut at 0.025. *Bottom:* Reflected and transmitted Love modes for an obliquely incident fundamental Rayleigh mode (angle of incidence: 25°).

wavenumbers satisfy Snell's law. The boundary conditions for $x_1 = 0$ express the continuity of displacements and stresses. At the same time, they define the reflection and transmission coefficients a^α and b^ν, respectively,

$$\begin{aligned} \tilde{U}_i + \sum_{\alpha=0}^{N_1} a^\alpha \tilde{U}_i^\alpha &= \sum_{\nu=0}^{N_2} b^\nu \tilde{U}_i^\nu + \tilde{U}_i, \\ \tilde{S}_{1i} + \sum_{\alpha=0}^{N_1} a^\alpha \tilde{S}_{1i}^\alpha &= \sum_{\nu=0}^{N_2} b^\nu \tilde{S}_{1i}^\nu + \tilde{S}_{1i}. \end{aligned} \tag{4}$$

The tilde characterizes non-normal incidence. By applying the rotation tensor on modes propagating in x_1 direction, it can be shown that for Rayleigh modes

$$\begin{aligned} \tilde{U}_1 &= \cos\varphi U_1, \quad \tilde{U}_2 = \sin\varphi U_1, \quad \tilde{U}_3 = U_3, \\ \tilde{U}_1^\alpha &= r^\alpha \cos\varphi^\alpha U_1^\alpha, \quad \tilde{U}_2^\alpha = \sin\varphi^\alpha U_1^\alpha, \quad \tilde{U}_3^\alpha = U_3^\alpha, \\ \tilde{S}_{11} &= \cos^2\varphi S_{11} + \sin^2\varphi S_{22}, \\ \tilde{S}_{12} &= \tfrac{1}{2}\sin(2\varphi)(S_{11} - S_{22}), \\ \tilde{S}_{13} &= \cos\varphi S_{13}, \\ \tilde{S}_{11}^\alpha &= \cos^2\varphi^\alpha S_{11}^\alpha + \sin^2\varphi^\alpha S_{22}^\alpha, \\ \tilde{S}_{12}^\alpha &= \tfrac{1}{2} r^\alpha \sin(2\varphi^\alpha)(S_{11}^\alpha - S_{22}^\alpha), \\ \tilde{S}_{13}^\alpha &= r^\alpha \cos\varphi^\alpha S_{13}^\alpha, \end{aligned} \tag{5}$$

and for Love modes

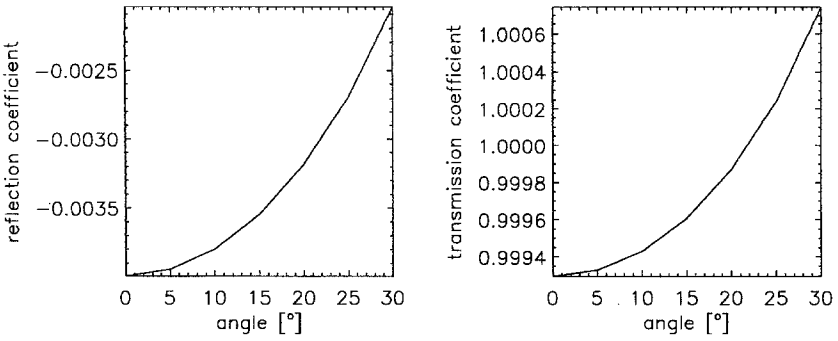

Figure 3. Reflection and transmission coefficients as a function of angle of incidence for the case of an incoming and outgoing fundamental Rayleigh mode for the model in Figure 1 on the bottom left for 83-sec period.

$$
\begin{aligned}
\tilde{U}_1 &= -\sin\varphi U_2, \quad \tilde{U}_2 = \cos\varphi U_2, \quad \tilde{U}_3 = 0,\\
\tilde{U}_1^a &= -\sin\varphi^a U_2^a, \quad \tilde{U}_2^a = r^a \cos\varphi^a U_2^a, \quad \tilde{U}_3^a = 0,\\
\tilde{S}_{11} &= -\sin(2\varphi)\, S_{12},\\
\tilde{S}_{12} &= \cos(2\varphi)\, S_{12},\\
\tilde{S}_{13} &= -\sin\varphi S_{23},\\
\tilde{S}_{11}^a &= -r^a \sin(2\varphi^a)\, S_{12}^a,\\
\tilde{S}_{12}^a &= \cos(2\varphi^a)\, S_{12}^a,\\
\tilde{S}_{13}^a &= -\sin\varphi^a S_{23}^a.
\end{aligned}
\tag{6}
$$

For reflected modes, the angle φ^a is the reflection angle. For transmitted modes, φ^a is the transmission angle. The angle of incidence φ and the transmission angle φ^a are the angles between the direction of propagation and the positive x_1 direction. For reflected modes, φ^a is the angle between the direction of propagation and the negative x_1 direction. By definition, all angles are positive. The quantity r^a is $+1$ for transmitted modes and -1 for reflected ones. For reflected and transmitted modes propagating non-normally in medium m, a modified orthogonality relation (Malischewsky, 1987)

$$
\frac{i\omega}{4r^a \cos\varphi^a}\int_0^\infty (\tilde{U}_j^a \tilde{S}_{1j}^{\beta *} - \tilde{U}_j^{\beta *}\tilde{S}_{1j}^a)\,dx_3 = \delta_{a\beta}, \quad \alpha,\beta = 0,\ldots,N_m \tag{7}
$$

holds. The residues $\tilde{U}_i$ and $\tilde{S}_{1i}$ in (4) summarize the contributions from neglected modes and body waves as well. Because of these residues, the reflection and transmission coefficients have to be approximated. If a finite set of discrete modes is considered, Malischewsky (1987) proposes to minimize

$$
F_2 = \int_0^\infty (\tilde{U}_i \tilde{S}_{1i}^* - \tilde{U}_i^* \tilde{S}_{1i})\,dx_3 \tag{8}
$$

to obtain approximated coefficients. Based on (8), in the following we formulate a linear system of equations for the approximation of reflection and transmission coefficients for a finite set of discrete propagating surface-wave modes. By taking the corresponding quantities from (4) and carrying out

$$
\begin{aligned}
\frac{\partial F_2}{\partial a^\alpha} &= 0, \quad \alpha = 0,\ldots,N_1,\\
\frac{\partial F_2}{\partial b^\nu} &= 0, \quad \nu = 0,\ldots,N_2,
\end{aligned}
\tag{9}
$$

we obtain, after some algebra, a symmetric and linear system of equations for the reflection and transmissions coefficients. By using (7), it can be written as

$$
\begin{aligned}
I_1^\alpha &= -\frac{4i}{\omega} a^\alpha \cos\varphi^\alpha + \sum_{\nu=0}^{N_2} b^\nu I_2^{\alpha\nu}, \quad \alpha = 0,\ldots,N_1,\\
-I_3^\nu &= \sum_{a=0}^{N_1} a^a I_2^{a\nu} + \frac{4i}{\omega} b^\nu \cos\varphi^\nu, \quad \nu = 0,\ldots,N_2
\end{aligned}
\tag{10}
$$

with

$$
\begin{aligned}
I_1^\alpha &= \int_0^\infty (\tilde{U}_i \tilde{S}_{1i}^{\alpha *} - \tilde{U}_i^{\alpha *}\tilde{S}_{1i})\,dx_3, \quad \alpha = 0,\ldots,N_1,\\
I_2^{\alpha\nu} &= \int_0^\infty (\tilde{U}_i^\alpha \tilde{S}_{1i}^{\nu *} - \tilde{U}_i^{\nu *}\tilde{S}_{1i}^\alpha)\,dx_3, \quad \alpha = 0,\ldots,N_1,\\
&\qquad\qquad \nu = 0,\ldots,N_2,\\
I_3^\nu &= \int_0^\infty (\tilde{U}_i \tilde{S}_{1i}^{\nu *} - \tilde{U}_i^{\nu *}\tilde{S}_{1i})\,dx_3, \quad \nu = 0,\ldots,N_2.
\end{aligned}
\tag{11}
$$

If mode index α of the reflected mode is equal to the index of the incident mode, I_1^α equals zero. The integration in (11) can be performed analytically for layers with constant properties. Inserting (5) and (6) in (11), the reflection and transmission angles appear in factors outside of the integration over depth. The system of equations (10) can be transformed into another one for a^α alone:

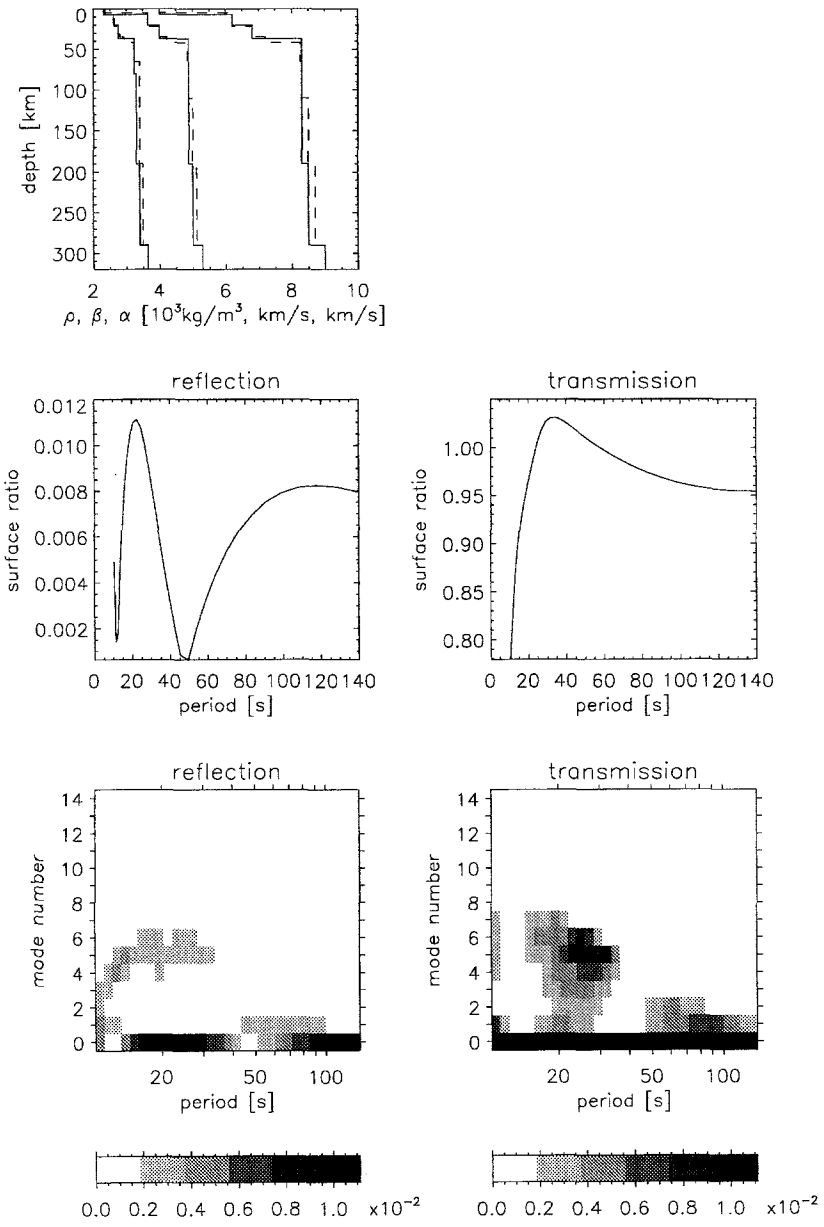

Figure 4. *Top:* Density, *S*- and *P*-wave velocity as a function of depth for a simplified model of the TTZ (profile LT-4); solid line, southwest of TTZ; dashed line, northwest of TTZ. *Middle:* Absolute value of surface ratios for reflection and transmission of the fundamental Rayleigh mode for perpendicular incidence of a fundamental Rayleigh mode. *Bottom:* Absolute value of surface ratios for reflected and transmitted Rayleigh modes as a function of period and mode for perpendicular incidence of a fundamental Rayleigh mode. Absolute values of surface ratio for the fundamental Rayleigh mode are cut at 0.0121.

$$I_1^\beta - \frac{i\omega}{4}\sum_{\nu=0}^{N_2}\frac{1}{\cos\varphi^\nu} I_2^{\beta\nu} I_3^\nu = i\sum_{\alpha=0}^{N_1} a^\alpha \left(-\frac{4}{\omega}\cos\varphi^\beta \delta_{\alpha\beta} + \frac{\omega}{4}\sum_{\nu=0}^{N_2}\frac{1}{\cos\varphi^\nu} I_2^{\alpha\nu} I_2^{\beta\nu}\right), \quad \beta = 0,\ldots,N_1, \tag{12}$$

and the transmission coefficients b^ν follow as

$$b^\nu = \frac{i\omega}{4\cos\varphi^\nu}\left(I_3^\nu + \sum_{\alpha=0}^{N_1} a^\alpha I_2^{\alpha\nu}\right), \quad \nu = 0,\ldots,N_2. \tag{13}$$

It should be noted that for non-normal incidence, the transmission coefficients can be greater than unity, because the energy flux fulfills (Malischewsky, 1987)

$$\sum_{\alpha=0}^{N_1}\frac{\cos\varphi^\alpha}{\cos\varphi}(a^\alpha)^2 + \sum_{\nu=0}^{N_2}\frac{\cos\varphi^\nu}{\cos\varphi}(b^\nu)^2 \leqq 1. \tag{14}$$

The equality sign in (14) holds for a complete mode set. We illustrate the approximation of the coefficients with a few examples. In each case, an incoming fundamental Rayleigh mode is considered. In Figure 1, we show how different depths of the lateral heterogeneity affect the frequency dependence of the reflection coefficient of the fundamental Rayleigh mode. Normal incidence of a fundamental Rayleigh mode is considered, and all propagating surface-wave modes up to the 14th higher Love and Rayleigh mode, if present, were taken into account to obtain reflection and transmission coefficients. A step of the Moho from 35 to 40 km yields maximal reflection coefficients for the fundamental mode for periods between 25 and 30 sec. For lateral

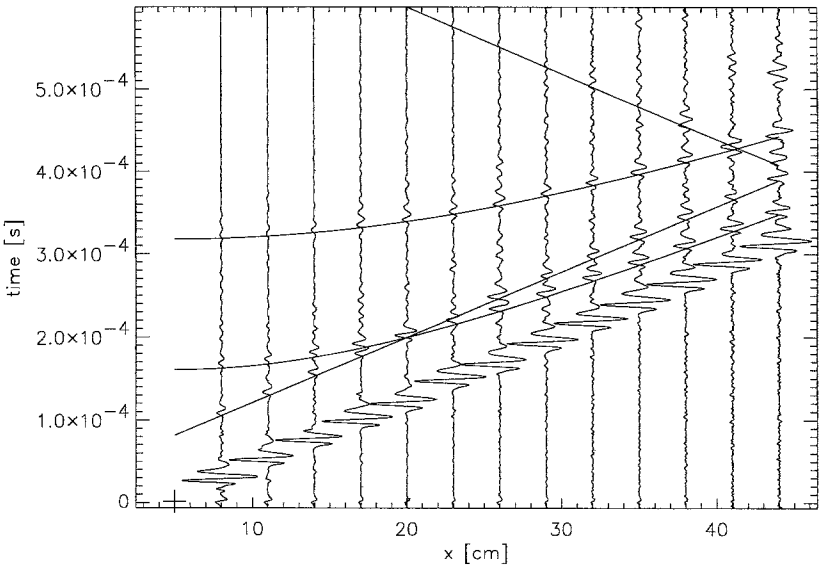

Figure 5. A profile of the ultrasonic experiment. Travel-time curves for Rayleigh modes reflected at the model edges are indicated.

changes in the lower lithosphere by 2%, the maximal absolute value of the reflection coefficient is obtained around 40 sec. If a lateral change by 2% is present in the asthenosphere, the maximal values occur between 60 and 120 sec period. In Figure 1 (*bottom*), a Moho step and lateral changes in the asthenosphere are combined. In this case, extremal values occur around 25 and 110 sec. Absolute values for reflection and transmission coefficients for the model on the bottom of Figure 1 are shown in Figure 2 for Rayleigh modes (*top*) and Love modes (*bottom*). Conversions to higher Rayleigh modes and for oblique incidence also to Love modes are likely. Conversions to reflected higher Rayleigh modes seem to be stronger if the reflection coefficient of the fundamental Rayleigh mode is small. Figure 3 shows an example for the dependence of the reflection and transmission coefficients on the angle of incidence. Moderate dependence on the angle of incidence is obtained for angles of incidence smaller than 30°. Finally, based on the results of Guterch *et al.* (1986) and Grabowska and Raczynska (1991), a simple model of the Tornquist–Teisseyre zone (TTZ) as a part of the Tornquist zone (TZ) was constructed combining different properties of this zone in one vertical discontinuity. Figure 4 presents the calculated surface ratios that contain the reflection and transmission coefficients and the displacements of the modes at the surface. Reflection coefficients up to 1% and mode conversion is expected at the TTZ according to this conservative estimate.

Algorithm for the Analysis of the Rayleigh-Wave Coda

In this section, an algorithm for the determination of reflection coefficients is developed. We are especially interested in determining reflection coefficients for discontinuities nearby a regional network using teleseismic events. Only the vertical components of fundamental Rayleigh modes are considered, and therefore, mode and component index are omitted. In principle, it is possible to extend the algorithm to the horizontal components and to a set of modes as well.

The model of the coda for a given source-station pair i, $i = 1, \ldots, N$, is

$$U_i = U_{i0} + \sum_{j=1}^{J} U_{ij}, \tag{15}$$

where U_{i0} is the direct wave and U_{ij} are reflected waves. Since multiple reflections are excluded, j is the index of the discontinuity. We may define a quantity G_{ij} that is

$$G_{ij} = \frac{U_{ij}}{U_{i0} R_j(\varphi_i)} \tag{16}$$

if the reflected wave reaches the station or zero otherwise. G_{ij} describes the additional propagation of the reflected wave to the discontinuity and from the discontinuity to the station in respect to the direct wave including geometrical spreading and damping and takes the different excitation of reflected and direct wave into account. The $R_j(\varphi_i)$ describe the unknown interactions with the discontinuities that in agreement to the previous section are assumed to be real. Using (16), equation (15) can be written as

$$U_i = U_{i0} + \sum_{j=1}^{J} U_{i0} G_{ij} R_j(\varphi_i) \tag{17}$$

or with deconvolution by an estimate of U_{i0}

$$D_i = \frac{U_i}{U_{i0}} = 1 + \sum_{j=1}^{J} G_{ij} R_j(\varphi_i). \tag{18}$$

It is possible to look at different narrow-frequency bands

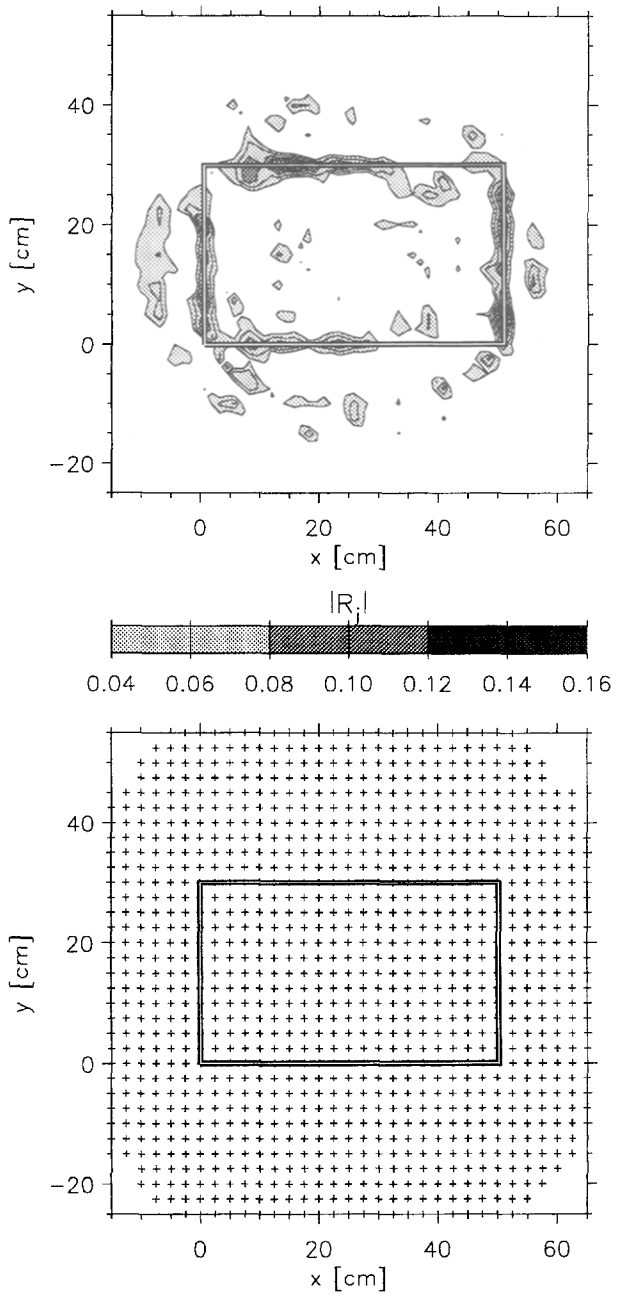

Figure 6. *Top:* Reconstruction of the model using reflected Rayleigh waves. Absolute values of the dimensionless interaction coefficients, $|R_j|$, are shown. On the axes, coordinates in centimeters are given. Model edges are indicated. *Bottom:* Sample points for which the R_j are determined.

separately by applying a set of filters $F(\omega_n)$ with different narrow-frequency windows in which the $R_j(\varphi_i)$ are assumed to be independent on frequency. The data D_i split up into a set of data $D_i(\omega_n)$:

$$D_i(\omega_n) = F(\omega_n) + \sum_{j=1}^{J} G_{ij}(\omega_n)R_j(\varphi_i,\omega_n). \qquad (19)$$

In the time domain and after applying a time window excluding the direct wave and containing the coda, we obtain

$$d_i(t,\omega_n) = \sum_{j=1}^{J} g_{ij}(t,\omega_n)R_j(\varphi_i,\omega_n). \qquad (20)$$

For the estimation of the $R_j(\varphi_i,\omega_n)$, the following two steps are carried out. First, we assume a large number of possible discontinuities J. For instance, discontinuities with different strikes may be attached to sample points of the region under consideration. Second, if the reflection points and the angles of incidence for different source-station pairs i and a given discontinuity j are similar, we assume the $R_j(\varphi_i,\omega_n)$ to be identical. Therefore, the number of unknowns decreases. If $G_{ij}(\omega_n)$ is modeled, equation (20) represents a linear system of equations for the determination of the unknown interactions $R_j(\varphi_i,\omega_n)$. It can be solved for different frequencies separately in a least-squares sense. The results are a function of ω_n. High values of $R_j(\varphi_i,\omega_n)$ indicate lateral heterogeneity. Small values should indicate lateral homogeneity. Considering the strike of a discontinuity obtained by the inversion and the directions of incoming and outgoing waves, it is possible to distinguish between reflections and refractions. If reflection occurs, the $R_j(\varphi_i,\omega_n)$ can be interpreted as estimates of reflection coefficients.

Ultrasonic Experiment

The algorithm was tested by an ultrasonic model experiment. A block of Plexiglas with dimensions 30 by 50 by 10 cm was used as a model. Eighty-eight records were obtained on five profiles parallel to the longest edge. The frequency band of the signals is 50 to 200 kHz. Figure 5 shows an example for records on the profile $y = 10$ cm. The Rayleigh fundamental mode can be recognized as the strongest onset. In the coda, single reflections from the edges of the model can be seen. The expected travel times are indicated by solid lines. The reflection of Rayleigh waves from a free vertical surface was investigated, for example, by Malischewsky (1976) and Fujii (1994). The absolute value of the reflection coefficient for normal incidence is approximately 0.2. It is larger than those presented in the first section. However, because of other strong waves than reflected Rayleigh waves in the coda, this experiment seems to be suitable for test purposes.

A lateral homogeneous background model was obtained with the help of which $g_{ij}(t,\omega_n)$ can be modeled. With several profiles similar to the one presented in Figure 5, we tried to reconstruct the lateral size of the model by using reflected Rayleigh waves. We attached a variable, R_j, to each sample point, neglecting the dependence of $R_j(\varphi_i)$ on the angle of incidence φ_i. In Figure 6 (*bottom*), the sample points are shown. They cover the model and a region around it. By solving equation (20), estimates for the R_j are obtained. Their absolute values are shown in Figure 6 (*top*). The borders of

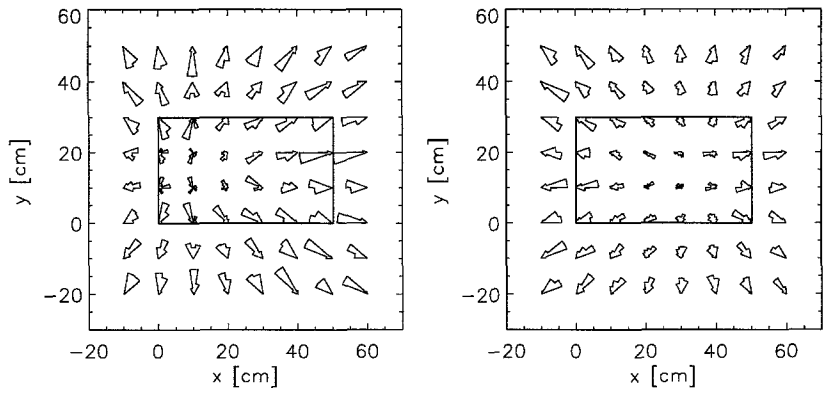

Figure 7. Frequencies of directions toward the sources (*left*) and the receivers (*right*). On the axes, coordinates in centimeters are given. Model edges are indicated.

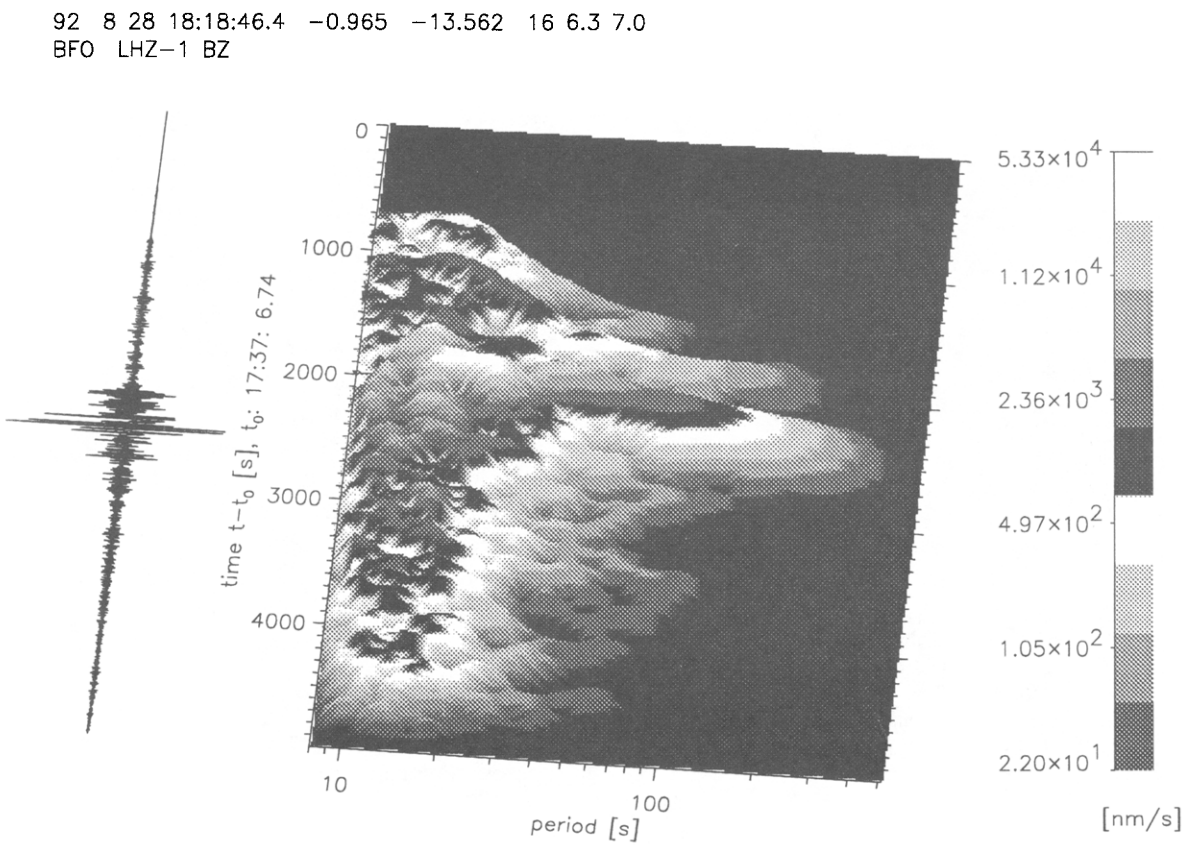

Figure 8. Amplitude calculated with the MFT as a function of period (x axis) and time (y axis) for the time series presented on the left, station BFO, and event specified in the title, after diminishing of the dispersion of the fundamental Rayleigh wave by convolution with an all-pass filter. Amplitudes are given in perspective representation. The largest values denote the Rayleigh fundamental mode. Its coda shows a decay with time and period and is visible up to 100-sec period.

the real model are indicated. Large values of $|R_j|$ refer to the reflecting edges of the model. The position of the model edges are reproduced very well. The recovered reflection coefficients are too small. One reason is that by assuming only one unknown per sample point, the angle dependence is neglected and the reflection coefficients are expected to be equal for each source-receiver pair that is an approximation in the case of reflections at a discontinuity. In principle, it is possible to allow for several unknowns at one sample point. Another reason is the nonuniqueness of the inversion.

Because of the arrangement of the sources and the receivers, the model is not recognized completely. For some sample points, Figure 7 shows frequencies of the directions to the sources (*left*) and to the transducers (*right*). For a reflection of the fundamental Rayleigh mode at a discontinuity, it is necessary that the angle of incidence is equal to the reflection angle. This is not met for the edges $y = 0$ cm

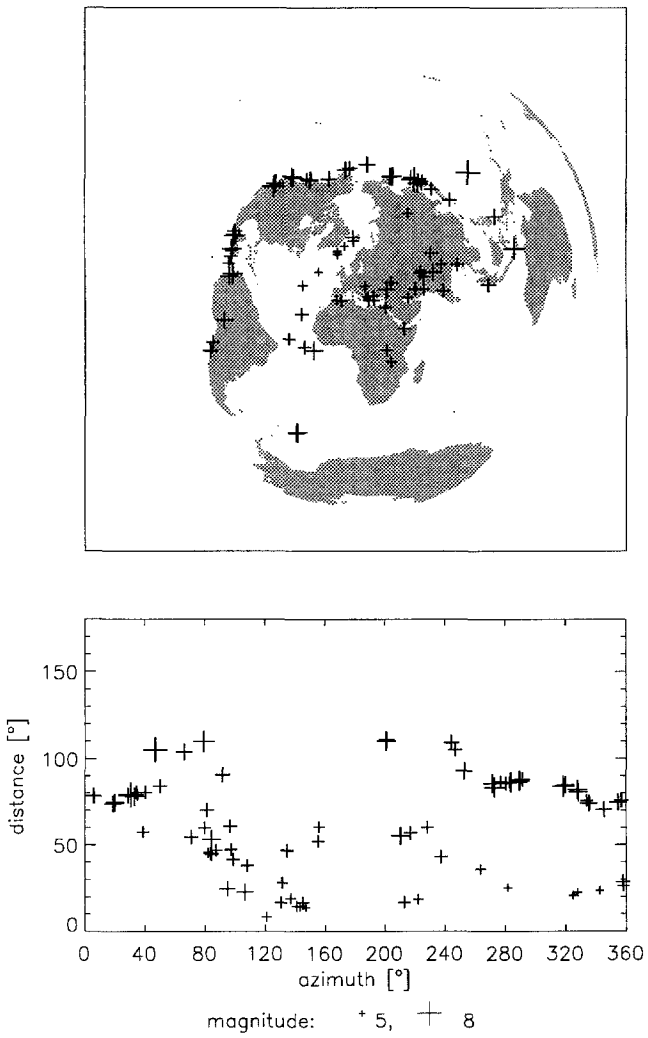

Figure 9. Epicenters of the events used in the inversion for $\omega_n = 25$ mHz. *Top:* Polar projection for a central point of the GRSN. *Bottom:* Azimuth and epicentral distance of the events. The size of the symbols indicates body-wave magnitude.

and $y = 30$ cm for x between $x = 35$ cm and $x = 50$ cm. It is obvious that the reconstruction of discontinuities depends on the configuration of the sources and the receivers in respect to the strike of the discontinuity.

Beside using $d_i(t,\omega_n)$, it is possible to invert its envelope. The advantage is that the spatial sampling rate can be decreased because the waveform becomes less sensitive to small changes in the position of the reflection point. But the relationship to the reflection coefficients can only be approximated with a linear model if only a few reflected waves are arriving at the station and no strong interferences are expected. The envelope is inverted in Figure 6.

Though not only reflected Rayleigh waves are present in the coda and only 88 traces are inverted, for this model and the given source-station configuration, the algorithm allows the imaging of lateral heterogeneity.

Application to Seismological Data in Central Europe

The conditions in an ultrasonic experiment, with an abundance of simple wave paths and with sharply defined boundaries, will be hard to match in seismology. However, the sharpness of boundaries in the Earth has been established for some tectonic lineaments. Although it is at present too early to apply the method to its full potential, we will present a preliminary application to real data in the region of Central Europe, where the GRSN is supplying low noise data and where the Tornquist–Teisseyre zone is very sharp (Zielhuis and Nolet, 1994).

Figure 8 shows in perspective representation the result of the multiple-filter technique (MFT) (Dziewonski and Hales, 1972) applied to a long-period recording of the vertical component at station BFO for an event specified in the title of Figure 8. The dispersion of the fundamental Rayleigh mode is diminished by convolution with an inverse all-pass filter. Therefore, dispersion can be neglected in narrow-frequency bands. The body waves show dispersion due to the deconvolution. The structure of the coda is very complicated especially for periods smaller than 30 sec. The coda of the fundamental Rayleigh wave shows a decay with time and period. It is weaker for periods larger than 30 sec, but it is visible up to 100 sec. The smallest represented value is greater than the noise. This can be seen comparing the coda to the noise before the first onset. The waves present in the coda cannot be identified as reflected fundamental Rayleigh waves in single seismograms. Refracted fundamental Rayleigh waves, scattered higher modes, and body waves contribute to the coda. Therefore, an inversion is applied to the coda that searches for reflected waves present in the coda of many seismograms and allows for waves other than fundamental Rayleigh waves reflected in the region under consideration.

Recordings mainly at stations of the GRSN were used for the inversion. They are supplemented by seismograms of a few stations nearby the GRSN (see Fig. 14 for location of the stations). For each of the studied 142 events, approximately 10 recordings were available. The maximum epicentral distance is 60° for 20°-sec period and 120° for periods larger than 60 sec. Figure 9 shows epicenters of events used in the inversion for $\omega_n = 25$ mHz and their distance and backazimuth for a central point of the GRSN.

The processing of the data includes a deconvolution of U_{i0} for a background model and the application of a set of filters with a Gaussian shape in the frequency domain (MFT). The filtered waveforms are inverted. Filtered seismograms are automatically selected for the inversion by applying the following criteria. The amplitude of the direct fundamental Rayleigh wave has to be larger than a given level (500 m/sec). Its measured group travel times for one event and different stations of a regional network should show a small variance after the deconvolution. The MFT allows for an estimation of the instantaneous frequency in narrow-frequency bands. For the fundamental Rayleigh wave, devia-

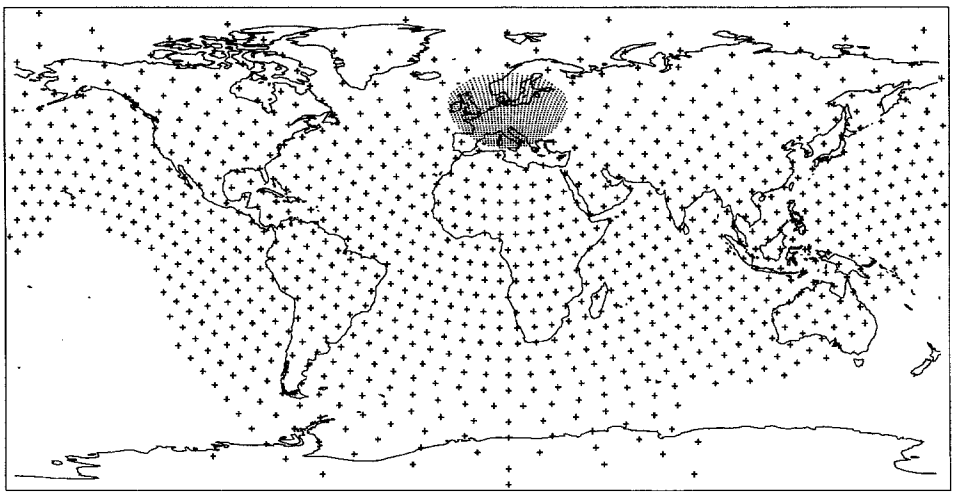

Figure 10. Sample points for the inversion, ω_n = 25 mHz. The region nearby the network shows a denser coverage.

tions of the measured frequency from the expected frequency, ω_n, have to be small. Finally, a time window is applied to the coda, and the amplitudes within the window are checked for unexpected high values. Depending on frequency, ω_n, between 200 and 700 seismograms were selected for the inversion. For about 25 mHz, most seismograms met the requirements.

The region nearby the stations is sampled, and unknowns $R_j(\omega_n)$ are attached to the sample points neglecting the angle dependence. To reduce the influence of waves not reflected within the region under consideration, sample points are also distributed outside of the region. Figure 10 shows sample points for ω_n = 25 mHz. Although sampling is less dense outside of the region under consideration, the complete paths are covered by sample points. Group travel times of the fundamental Rayleigh wave remaining after the deconvolution of a background model are measured. Using these measurements and a laterally homogeneous background model for the region under consideration (Dost, 1990), the $g_{ij}(t,\omega_n)$ are approximated neglecting the dispersion within the narrow-frequency band denoted by ω_n. Equation (20) is solved for different ω_n.

The TZ in Central Europe consists of the Sorgenfrei–Tornquist zone (STZ) in the NW and the TTZ in the SE (Berthelsen, 1992). The TZ is part of a complex transition zone between ancient Europe (Baltica) with intact Precambrian basement and Variscan Central Europe. It is assumed that the basement of Baltica thinned during Palaezoic and Mesozoic, and extends beyond the STZ to northern Germany. During Late Cretaceous and Early Tertiary, Alpine-induced inversion affected the TZ. The intensity of the inversion increases from the NW to the SE (Berthelsen, 1992).

Figure 11 shows absolute values of estimated interaction coefficients $|R_j(\omega_n)|$ as a function of period for two profiles crossing the TZ, namely, the NW of (a) the TTZ and (b) the STZ. Estimates of $|R_j(\omega_n)|$ for 20 different periods contribute to these profiles. The maximal resolution is obtained between 20- and 40-sec period. The corresponding depth range is estimated using theoretical reflection coefficients like in Figure 1. Lateral heterogeneity approximately between 15 and 50 km depth is imaged. For latitudes larger than 53° N, the profile (a) shows properties of Baltica's lithosphere. A change in the structure occurs at about 53° N where the profile crosses the TTZ. Between 51° N and 53° N, profile (a) corresponds remarkably well to an about 200-km-wide zone of thinned crust SW of the TTZ described in Guterch *et al.* (1994) based on refraction and wide angle reflections for the profile LT-7. In profile (a), strong lateral heterogeneity is found at 50.5° N for periods smaller than 27 sec. It can be interpreted as lateral changes in the lower crust at the Elbe Lineament (EL). Strong lateral heterogeneity at the Elbe Lineament is present also on profile (b). This corresponds to anomalous low velocities in the lower crust found in refraction and wide-angle reflection recordings along EUGENO-S line 1 (EUGENO-S Working Group, 1988; Ansorge *et al.*, 1992). Southwest-dipping lateral heterogeneity may be present between 57° N and 55° N in 20 to 30 km depth between the STZ and the Ringkøbing-Fyn High. This is partly supported by a lateral velocity decrease toward SW between 10 and 25 km depth described by Ansorge *et al.* (1992). Also interesting is the low heterogeneity between 52.5° N and 55.5° N for periods between 25 and 30 sec in profile (b). This period range shows maximum sensitivity for about 35 to 40 km depths. For the same latitudes and periods larger than 35 sec, a NE-dipping heterogeneity is found. These structures need validation by further studies. The profiles clearly show similarities to results of seismic studies by considering the relation between depth of the heterogeneity and periods of maximum sensitivity of reflection coefficients. However, this relation may be masked by local extrema and zeros in the curves of reflection coefficients as a function of period. Because of the smaller absolute values

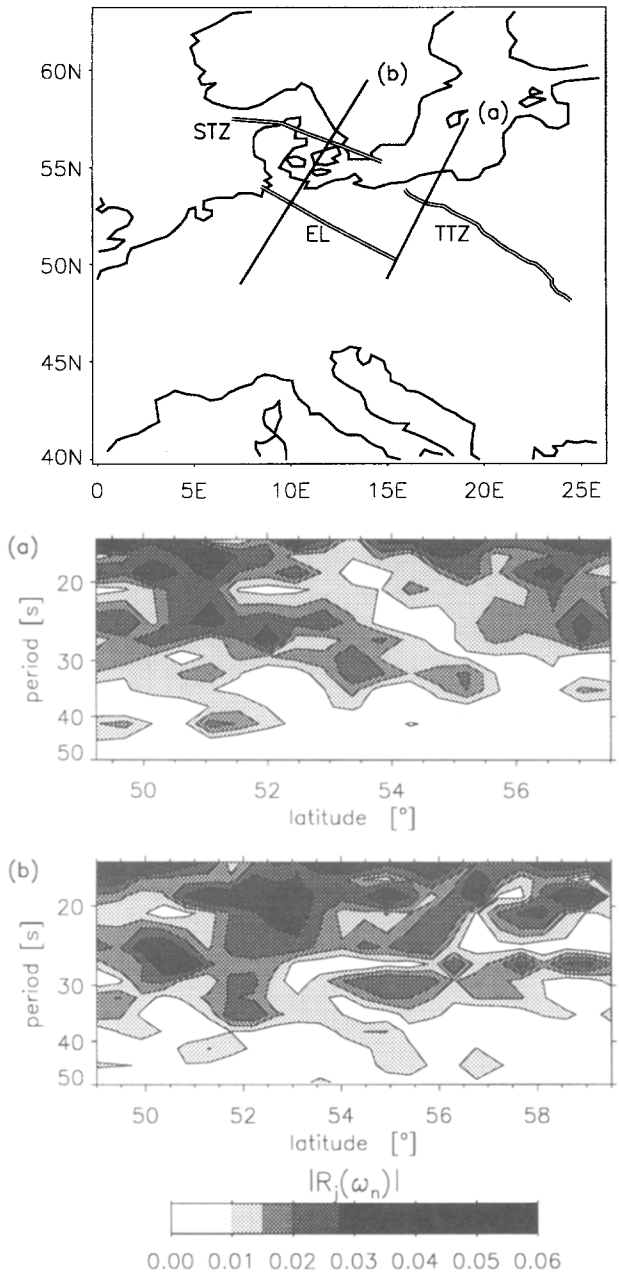

Figure 11. Reflection of the fundamental Rayleigh mode, $|R_j(\omega_n)|$, as a function of period for two profiles crossing (a) the TTZ and (b) the STZ. The map shows coastlines for Central Europe, the profiles, and some tectonic lines (STZ, Sorgenfrei–Tornquist zone; TTZ, Tornquist–Teisseyre zone; EL, Elbe lineament). The $|R_j(\omega_n)|$ along the profiles are given as a function of latitude (x axis) and period (y axis).

of local extrema, the application of a depth-period relation seems to be justified.

An inversion for a broader frequency range (30- to 50-sec period) is carried out although the $R_j(\omega_n)$ are strongly frequency dependent. The $R_j(\omega_n)$ are assumed to be constant in that frequency band. Absolute values of the resulting $R_j(\omega_n)$ are shown in Figure 12. There is a tendency toward smaller amplitudes with increasing distance from the region of dense station coverage (see Fig. 14 for station locations). The time window applied on the waveform of the coda does not allow for small time delays of reflected waves in respect to the fundamental Rayleigh wave. Because for regions with high station coverage small delay times are typical, the coverage in the inversion is low (see Fig. 13). The smaller amplitudes are probably due to the higher coverage in the inversion and simplifications in the method. Periods from 30 to 50 sec are sensitive to lateral changes in crustal thickness and lateral heterogeneity within the lower crust and the uppermost mantle.

Remarkable in Figure 12 is a zone of high values slightly NE of the TTZ. The offset is most likely due to a somewhat too high group velocity used in the inversion. This can be explained by a too fast background model, or periods shorter than 40 sec dominate the inversion result. The group velocity is smaller for these periods than the group velocity for 40 sec used in the inversion. Lateral heterogeneity for the TTZ is in agreement to Snieder (1988), who shows that surface waves are scattered at the TTZ. Zielhuis and Nolet (1994) detect lateral changes perpendicular to the TZ up to 5% in the NW and up to 12% in the SE of the TZ.

Figure 12 can be compared to crustal thickness in Central Europe (Giese, 1995). Regions with high lateral gradients in crustal thickness show high values in Figure 12. High values around the Bohemian Massif (BM) and for the Upper Rhine Graben (URG) can be explained by enlarged (34 km) and decreased (25 km) crustal thickness, respectively. The Lüneburg Massif (LM) (Berthelsen, 1992) in NW Germany shows 32-km crustal thickness in contrast to 28 km and lower beneath the North Sea (Giese, 1995). Less-pronounced zones of high $|R_j(\omega_n)|$ in Figure 12 correspond to enlarged crustal thickness for the Ringkøbing-Fyn High (EUGENO-S Working Group, 1988) and the Alps (Ansorge *et al.*, 1992). Lateral heterogeneity along the STZ is not continuous. This may be explained by varying lateral gradients in crustal thickness found by EUGENO-S Working Group (1988). High values for the Variscan Rheno-Herzynian Saxo-Thuringian boundary (Central European Suture, CES) and the Elbe Lineament are probably due to lateral changes within the crust and the uppermost mantle. Lateral velocity changes in the lower crust for the Elbe Lineament are described by Ansorge *et al.* (1992) and Bankwitz (1993). Regions between Elbe Lineament and TTZ show apparently low lateral heterogeneity.

In Figure 13, frequencies of the directions toward the sources and the stations for sample points in the region under consideration are given. For the region under consideration, the angles between these two directions are smaller than 90°. Single refractions at a discontinuity are characterized by angles larger than 90°. Therefore, for the region under consideration, we search for backscattered waves that can be interpreted in terms of reflections if a lateral discontinuity is

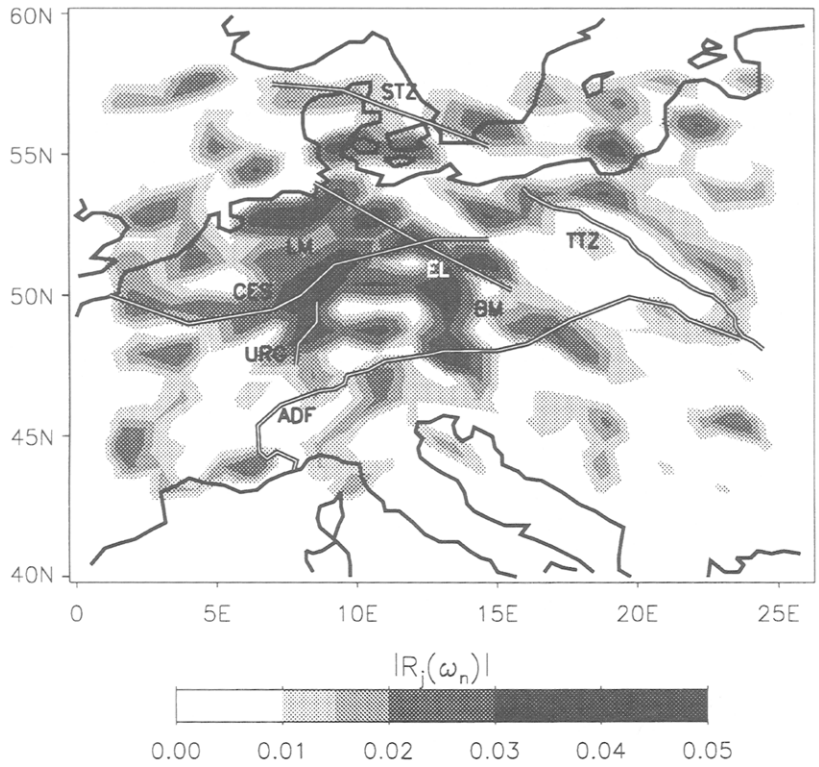

Figure 12. Reflection of the fundamental Rayleigh mode, $|R_j(\omega_n)|$, for a band pass from 30- to 50-sec period projected on a map of Central Europe. Coastlines and tectonic lines are given (STZ, Sorgenfrei–Tornquist zone; TTZ, Tornquist–Teisseyre zone; EL, Elbe lineament; LM, Lüneburg Massif; CES, Central European Suture (Variscan Rheno-Herzynian Saxo-Thuringian boundary); URG, upper Rhine graben; BM, Bohemian Massif; ADF, Alpine deformation front).

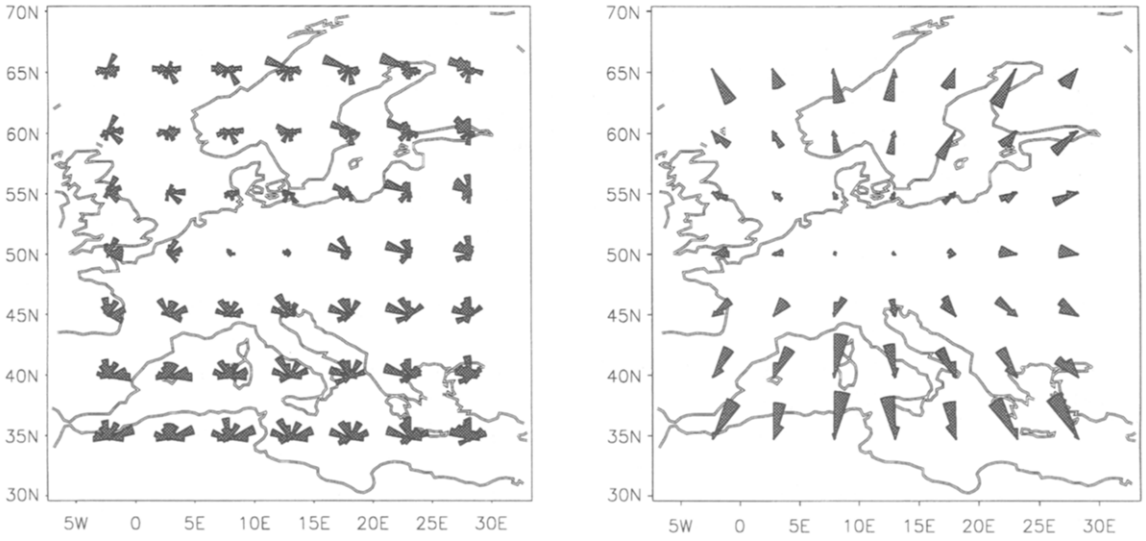

Figure 13. Frequencies of source azimuths (*left*) and station azimuths (*right*) for ω_n = 25 mHz and sample points in Central Europe.

present. Outside of the region under consideration, the angle can be larger than 90°, so that here sample points can account for single reflections and single refractions. In Figure 13, the incoming waves approach the sample points from a wide range of azimuths. Neglecting the angle dependence is a simplification. The model experiment confirms the possibility to neglect the angle dependence of the reflection. Only discontinuities with a strike that allows for reflections can be detected. Especially, discontinuities striking toward the stations cannot be imaged. Note the lower coverage for sample points nearby the stations.

A synthetic spike test for the horizontal resolution is shown in Figure 14 using the same source and receiver configuration as for real data. Synthetic waveforms for scatterers with $R_j(\omega_n) = 1$ were calculated and inverted. The location is reproduced, but amplitudes are too small, and weak artifacts due to the nonuniqueness of the inversion are visible. Lateral resolution is about 200 km.

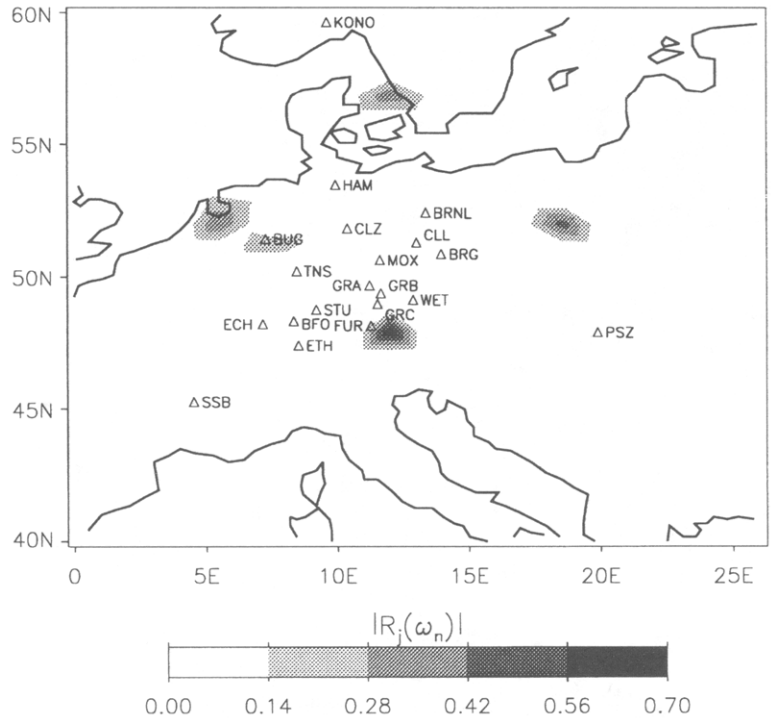

Figure 14. Synthetic spike test for horizontal resolution of the inversion, $\omega_n = 25$ mHz. Coast lines of Central Europe are given. Stations are denoted by triangles.

Conclusions

A method for the determination of approximate reflection and transmission coefficients of surface waves for a given vertical discontinuity is considered. It yields coefficients for a finite set of discrete propagating surface-wave modes. Non-normal incidence and mode conversion between Love and Rayleigh modes can be studied. For vertical discontinuities, a relation is found between the depth of lateral heterogeneity and the period range of enlarged absolute values of reflection coefficients. In the given examples, reflection coefficients of the fundamental Rayleigh mode for periods up to 40 sec are sensitive to the crust. Between 30 and 80 sec, they are sensitive to the lithospheric mantle, and between 50 and 120 sec, to the asthenosphere.

The complicated structure of the fundamental Rayleigh-wave coda is confirmed by analyzing seismograms with the multiple-filter technique. The coda shows a decay with time and period and is for strong events visible up to 100 sec. The Rayleigh-wave coda was studied for single reflected fundamental Rayleigh waves. Refractions can show large amplitudes (see Figs. 2 and 3) and contribute to the coda. Refractions with small delay times are excluded from the inversion by a time window. The arrival of the fundamental Rayleigh wave is measured in dependence on frequency. The time window of the inversion starts with a frequency-dependent offset after the arrival of the fundamental Rayleigh wave. For 25 mHz, the offset is 200 sec. For the region under consideration, the angles between the directions to the sources and to the stations (see Fig. 13) are smaller than 90°. Here, the inversion tries to find single backscattered waves or reflected waves if a discontinuity is present. The sample points outside the region under consideration covering the complete paths can account for single refractions and reflections. Because of these sample points, the coda waveform is only partially explained in terms of fundamental Rayleigh waves reflected in the region under consideration. A complicating fact is that body waves, higher modes, multiple reflections, and refractions contribute to the coda. Because of low coverage and simplifications in the algorithm, artificial anomalies may occur or heterogeneity may not be imaged. The similarities to lateral gradients in maps of Moho depths and results of deep seismic soundings confirm the applicability of the method. For periods between 20 and 50 sec, the inversion of the coda waveform images possible scatterers and reflectors of surface waves. It is confirmed that surface waves are reflected at intraplate structures like the TTZ, and strong lateral heterogeneity is found for the Elbe Lineament in the lower crust. The results are encouraging for an incorporation of scattering into tomographic inversions using surface waves for periods between 20 and 50 sec.

Acknowledgments

This work was supported by the Deutsche Forschungsgemeinschaft, Bonn, under Grant Number Ma 1520/2-2. We thank Prof. E. Wielandt, University Stuttgart, for the discussions, for computer routines, as well as the technical know-how for the model experiment. Furthermore, we thank Prof. G. Nolet and Dominique Gillard, Princeton University, for helpful discussions, and Dipl.-Ing. A. Ziegert, University Jena, for technical support in carrying out the model experiment. We thank A. Levshin and an anonymous reviewer for their suggestions.

PGM dedicates this article to the memory of his mother, Alice Malischewsky.

References

Aki, K. and B. Chouet (1975). Origin of coda waves: source, attenuation and scattering effects, *J. Geophys. Res.* **80,** 3322–3342.

Alsop, L. E. (1966). Transmission and reflection of Love waves at a vertical discontinuity, *J. Geophys. Res.* **71,** 3969–3984.

Ansorge, J., D. Blundell, and St. Mueller (1992). Europe's lithosphere—seismic structure, in *A Continent Revealed—The European Geotraverse,* D. Blundell, R. Freeman, and S. Mueller (Editors), University Press, Cambridge, 33–69.

Bankwitz, P. (1993). Crustal types of eastern Central Europe, *Publications of the Institute of Geophysics, Polish Academy of Sciences A-20* **255,** 13–17.

Berthelsen, A. (1992). From Precambrian to Variscan Europe, in *A Continent Revealed—The European Geotraverse,* D. Blundell, R. Freeman, and S. Mueller (Editors), University Press, Cambridge, 153–164.

Dost, B. (1990). Upper mantle structure under western Europe from fundamental and higher mode surface waves using the NARS array, *Geophys. J. Int.* **100,** 131–151.

Dziewonski, A. M. and A. L. Hales (1972). Numerical analysis of dispersed seismic waves, in *Methods in Computational Physics,* Vol. 11, B. A. Bolt (Editor), Academic Press, New York.

EUGENO-S Working Group (1988). Crustal structure and tectonic evolution of the transition between the Baltic Shield and the North German Caledonides (the EUGENO-S Project), *Tectonophysics* **150,** 253–348.

Fujii, K. (1994). Rayleigh-wave scattering at various wedge corners: investigation in the wider range of wedge angles, *Bull. Seism. Soc. Am.* **84,** 1916–1924.

Giese, P. (1995). Main features of geophysical structures in Central Europe, in *Pre-Permian Geology of Central and Eastern Europe,* R. D. Dallmeyer, W. Franke, and K. Weber (Editors), Springer, Berlin, 7–25.

Grabowska, T. and M. Raczynska (1991). Structure of the Earth's crust on the Polish Lowland in the light of gravimetric modelling, *Publications of the Institute of Geophysics, Polish Academy of Sciences A-19* **230,** 85–110.

Gregersen, S. and L. E. Alsop (1974). Amplitudes of horizontally refracted Love waves, *Bull. Seism. Soc. Am.* **64,** 535–553.

Guterch, A., M. Grad, R. Materzok, and E. Perchuc (1986). Deep structure of the Earth's crust in the contact zone of the Palaeozoic and Precambrian platforms in Poland (Tornquist-Teisseyre Zone), *Tectonophysics* **128,** 251–279.

Guterch, A., M. Grad, T. Janik, R. Materzok, U. Luosto, J. Yliniemi, E. Lueck, A. Schulze, and K. Foerste (1994). Crustal structure of the transition zone between Precambrian and Variscan Europe from new seismic data along LT-7 profile (NW Poland and eastern Germany), *Comptes Rend. Acad. Sci.* **319,** serie II, (7), 1489–1496.

Hanka, W. (1990). The German Regional Broadband Seismic Network (GRN) Project, in *Workshop on MedNet,* E. Boschi, D. Giardini, and A. Morelli (Editors), Instituto Nazionale di Geofisica, Roma, 83–95.

Its, E. N. and T. B. Yanovskaya (1985). Propagation of surface waves in a half-space with vertical, inclined or curved interfaces, *Wave Motion* **7,** 79–84.

Keilis-Borok, V. I. (Editor) (1989). *Seismic Surface Waves in a Laterally Inhomogeneous Earth,* Kluwer Acad. Publ., Dordrecht.

Kennett, B. L. N. (1984). Guided wave propagation in laterally varying media—I. Theoretical development, *Geophys. J. R. Astr. Soc.* **79,** 235–255.

Levshin, A. (1985). Effects of lateral inhomogeneities on surface waves amplitude measurements, *Ann. Geophys. B.* **3,** 511–518.

Levshin, A. and K. A. Berteussen (1979). Anomalous propagation of surface waves in the Barents Sea as inferred from NORSAR recordings, *Geophys. J. R. Astr. Soc.* **56,** 97–118.

Malischewsky, P. (1976). Surface waves in media having lateral inhomogeneities, *Pure Appl. Geophys.* **114,** 833–843.

Malischewsky, P. (1979). An improvement of Alsop's method for the determination of reflection and transmission coefficients of surface waves, *Pure Appl. Geophys.* **117,** 1045–1049.

Malischewsky, P. (1987). *Surface Waves and Discontinuities,* Elsevier, Amsterdam.

Maupin, V. and B. L. N. Kennett (1987). On the use of truncated model expansions in laterally varying media, *Geophys. J. R. Astr. Soc.* **91,** 837–851.

Sato, R. (1961). Love waves propagated across transitional zone, *Jap. J. Geophys.* **2,** 117–134.

Snieder, R. (1986). 3-D Linearized scattering of surface waves and a formalism for surface wave holography, *Geophys. J. R. Astr. Soc.* **84,** 581–605.

Snieder, R. (1988). Large-scale waveform inversions of surface waves for lateral heterogeneity, 2. Application to surface waves in Europe and the Mediterranean, *J. Geophys. Res.* **93,** 12067–12080.

Snieder, R. and G. Nolet (1987). Linearized scattering of surface waves on a spherical Earth, *J. Geophys.* **61,** 55–63.

Stange, St. and W. Friederich (1992). Guided wave propagation across sharp lateral heterogeneities: the complete wavefield at plane vertical discontinuities, *Geophys. J. Int.* **106,** 183–190.

Zielhuis, A. and G. Nolet (1994). Deep seismic expression of an ancient plate boundary in Europe, *Science* **265,** 79–81.

Institute of Geosciences
Friedrich-Schiller University Jena
Burgweg 11
D-07749 Jena, Germany
E-mail: pet@rz.uni-jena.de
(T. M.)

Institute of Geosciences
Friedrich-Schiller University Jena
Burgweg 11
D-07749 Jena, Germany
E-mail: mali@geo.uni-jena.de
(P. G. M.)

Stauffenbergstr. 11
D-07747 Jena, Germany
(H. N.)

Manuscript received 25 January 1996.